Theory of Phase Behavior of Poly(oxyethylene)−Poly(oxypropylene)−Poly(oxyethylene) Triblock Copolymers in Aqueous Solutions

Jaan Noolandi* and An-Chang Shi

Xerox Research Centre of Canada, 2660 Speakman Drive, Mississauga, Ontario, Canada L5K 2L1

Per Linse

Physical Chemistry 1, Center for Chemistry and Chemical Engineering, Lund University, P.O. Box 124, S-221 00 Lund, Sweden

Received February 20, 1996; Revised Manuscript Received June 10, 1996[⊗]

ABSTRACT: The phase behavior of ABA triblock copolymers in aqueous solutions is studied theoretically, using both continuum and lattice mean-field theories. A variety of lyotropic liquid crystalline phases is found for the Pluronic family, and the effects of temperature, copolymer concentration, overall molecular weight, and block sizes are investigated. The theoretical scheme incorporates "internal" monomeric states as well as the effects of the spatial arrangement of the molecules and may be viewed as a generalization of the traditional theory of ordered phases in block copolymers. The interaction parameters determined for poly(oxyethylene) and poly(oxypropylene) homopolymers in aqueous solutions are found to give good agreement for the theoretically predicted ordered structures when compared with measurements on different Pluronic polymers using ^{2}H NMR of deuterated water and small-angle X-ray scattering.

I. Introduction

An unusual feature of EO−PO−EO (EO, ethylene oxide; PO, propylene oxide) triblock copolymers (trade name Pluronic) in water is the variety of liquid crystalline phases that can form over a relatively narrow temperature range (∼50 °C).[1−3] These copolymers, which are denoted by $(EO)_n(PO)_m(EO)_n$, where *n* and *m* represent the number of EO and PO units, respectively, consist of a central hydrophobic block (PO) and two hydrophilic end blocks (EO). The lengths of the EO and PO blocks as well as their relative sizes have a marked effect on the mesomorphic behavior of the block copolymers in aqueous solution. In addition, the rapid decrease of the hydrophilic nature of the EO and PO blocks with increasing temperature and the concentration dependence of the copolymer in solution are important factors affecting the phase behavior.

Over the last few years, the effects of temperature on the phase equilibria and structure of poly(ethylene oxide) copolymers in water have been extensively studied using ^{2}H NMR,[4] and more recently SAXS,[5] to characterize the nature of the lyotropic liquid crystalline phases. This work has been paralleled by detailed studies of the homopolymer−water binary phase diagrams for both the ethylene oxide and propylene oxide homopolymers in order to determine the monomer−monomer and monomer−solvent interaction parameters and to provide a quantitative description of the change in hydrophobic/hydrophilic behavior of the homopolymers with changing temperature.[6] The micellar structure of a dilute solution of the triblocks in water has been well described by a theoretical model[7,20] based in part on the analysis of the binary homopolymer−water phase behavior.

In this paper we apply a self-consistent mean-field theory (in both the lattice and continuum versions) to calculate the relative stability of the self-assembled liquid crystalline phases (cubic, hexagonal, lamellar) for some representative systems and a range of external parameters. This work draws heavily on earlier theoretical and experimental studies dealing with homopolymers and micelle.[6,7] However, for triblock copolymers, the connectivity of the molecules, the subtle interplay of the entropic changes due to chain stretching and localization, the free energy cost of forming interfaces, and the selective partitioning of the solvent into the ordered domains add a new dimension to the challenge of predicting the phase behavior and understanding the main tendencies that underlie the complexity of the experimental observations.

Although triblock copolymer surfactants of ethylene oxide and propylene oxide have a wide range of uses as emulsifiers, wetting agents, solubilizers, etc.,[8] we do not focus on any particular application in this paper. However, the theoretical analysis developed here, and its extensions to include organic solvents[9] and interactions with surfaces, should be of value for predicting thermodynamic behavior in specific practical situations. In addition, the theoretical infrastructure should be helpful in developing more detailed models for nonionic polymeric systems with hydrophobic and/or hydrophilic modifications, and one can make use of analogous theoretical studies[10,11] relating to mixtures of random copolymers, homopolymers, and block copolymers with and without selective organic solvents.

The paper is organized as follows. Section II contains a summary description of the theoretical model, with separate descriptions of the continuum and lattice approaches to the self-consistent mean-field theory. It is evident that there is a close connection between the two descriptions, which become formally equivalent for long chain lengths. The micelle model as used by Linse[7] within the lattice description is also summarized, and a translation table for some equivalent quantities in the two theories is given. Section III presents the calculated phase diagrams for a selection of Pluronic polymers for studying the effect of changing the weight percent of poly(ethylene oxide) while keeping the molecular weight of poly(propylene oxide) constant, as well as changing

[⊗] Abstract published in *Advance ACS Abstracts,* July 15, 1996.

S0024-9297(96)00272-0 CCC: $12.00

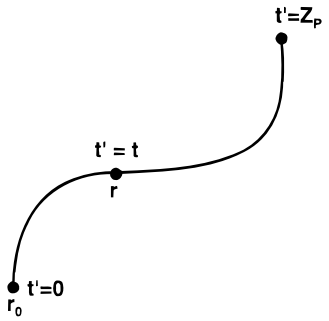

Figure 1. Schematic of a space curve implicit in the expression for the Green function $Q_p(\mathbf{r}, t|\mathbf{r}_0)$ (eq 1 in text) representing the configuration of a homopolymer with one end ($t' = 0$) at $\mathbf{r}_0$, total length $t' = Z_p$, and the contour length corresponding to t passing through point $\mathbf{r}$.

the molecular weight of poly(propylene oxide) while keeping the weight percent of poly(ethylene oxide) constant. The density profiles for one system (P94) are studied in detail for two different temperatures and three different morphologies (hexagonal, lamellar, inverse hexagonal), and the junction distributions are calculated and related to the expected change in the shear modulus for P94 as a function of temperature. Section IV contains the conclusions with respect to the systems studied, as well as some comments about the theoretical approaches.

II. Theoretical Model

We use a mean-field description of inhomogeneous polymeric systems and apply the theory in two different versions, the continuum model as derived from the functional integral formalism of Edwards[12] and the lattice model as extended and developed by Scheutjens and Fleer[13] from the earlier work by Flory.[14] The common element in both cases is the mean-field assumption, and the two models are formally equivalent in this respect. The micelle model as developed by Scheutjens and co-workers (subsection C) is applied only within the lattice framework. The ordered block copolymer phases are studied using both the continuum and lattice models. We begin with a description of the continuum model.

A. Continuum Description. The partition function for a multicomponent polymer blend, including a solvent, is given as a functional integral over all space curves representing the polymer chains. As shown by Hong and Noolandi,[15] the mean-field approximation is obtained by performing the functional integral using the saddle function method (taking the maximum of the integrand) with the constraint of local incompressibility of the polymer mixture. The result of this procedure is a modified diffusion equation for the primary quantity of interest, the Green function $Q_p(\mathbf{r}, t|\mathbf{r}_0)$, which represents the distribution function of a polymer p with one end at $\mathbf{r}_0$ and the position along the chain corresponding to the contour length t at $\mathbf{r}$, while the rest of the chain, from the contour length t to the full contour length Z_p, is elsewhere.[16] The mean field in the modified diffusion equation is given in terms of integrals over the distribution functions of all the components of the system (including the solvent), and the problem must be solved self-consistently using a numerical method described previously.[15] The labeling scheme of the space curves for the Green function $Q_p(\mathbf{r}, t|\mathbf{r}_0)$ is shown in Figure 1.

In what follows we will obtain the new result that a polymer model with internal degrees of freedom[17] can be described in terms of an effective mean-field potential derived from the partition function of the internal states embedded in an external field. This model, in which the internal degrees of freedom are populated according to a Boltzman distribution independently of the physical arrangement of the polymer chains, has previously led to a successful description of the inverse temperature behavior of homopolymers in homogeneous[6,17−19] and heterogeneous systems.[7,20−22] For the specific case of interest here, the model takes into account that different conformations of the ethylene oxide groups differ in their dipole moments and that the more polar conformations are less numerous. The conformations are divided into two classes or states, one being more polar with a lower energy and a lower statistical weight and one being less polar (referred to as nonpolar), having a higher energy and higher statistical weight. This categorization is also consistent, e.g., with ^{13}C chemical shift measurements.[23] At low temperatures, the former class dominates and the effective polymer−solvent interaction is favorable, whereas at higher temperatures the latter class dominates, rendering the polymer−solvent interaction less favorable. Furthermore, the effective polymer−solvent interaction becomes more unfavorable as the polymer concentration increases. The formalism is also applied to propylene oxide groups. Poly(propylene oxide) displays similar inverse temperature behavior as poly(ethylene oxide).

In order to include the internal degrees of freedom, as described above, into the continuum mean-field model for homopolymers, it is most expedient to start from the formal expression for the Green function,

$$Q_p(\mathbf{r}, t|\mathbf{r}_0) = \int_{\mathbf{r}_p(0)=\mathbf{r}_0}^{\mathbf{r}_p(t)=\mathbf{r}} \delta\mathbf{r}_p(\bullet) P(\{\mathbf{r}_p(\bullet)\}) \exp\{-\int_0^{Z_p} dt' \omega_p[\mathbf{r}_p(t')]\} \quad (1)$$

where the functional integral is over all the space curves $\mathbf{r}(\bullet)$ which represent the possible configurations of the macromolecule consistent with the constraints indicated in Figure 1, where one end ($t' = 0$) of a homopolymer is at $\mathbf{r}_0$ and the contour length corresponding to t is at $\mathbf{r}$.[16] As usual for flexible polymers, the probability functional for a given space curve $P(\{\mathbf{r}_p(\bullet)\})$ is assumed to be the Wiener form,[12]

$$P(\{\mathbf{r}_p(\bullet)\}) \propto \exp\left\{-\int_0^{Z_p} dt' \frac{3}{2b^2}\dot{\mathbf{r}}_p^2(t')\right\} \quad (2)$$

where b is taken to be the Kuhn statistical length of a single segment of the polymer chain. The "potential" $\omega_p[\mathbf{r}_p(t')]$ is introduced formally (through the integral representation of the spatial δ function for the chain contours) as a conjugate field for the density of polymer p. Although $Q_p(\mathbf{r}, t|\mathbf{r}_0)$ satisfies a modified diffusion equation in the "potential" $\omega_p[\mathbf{r}_p(t')]$, the analysis becomes tractable only when the mean-field approximation is made, and ω_p can be written as an explicit function of all the polymer densities, taking into account the local incompressibility of the polymer mixture.[15]

Considering the internal states of a segment of polymer p, the state partition function becomes

$$\sum_\alpha g_{p\alpha} \exp\{-\beta E_{p\alpha}\} \quad (3)$$

where $E_{p\alpha}$ is the internal energy and $g_{p\alpha}$ the statistical weight of the segment in state α. These parameters

Table 1. Internal State Parameters (E_{AB} and g_{AB}) and Flory−Huggins Interaction Parameters ($\chi_{BB'}$) of the Theoretical Model (Energy in kJ mol^{-1})

species	state	state no.	E_{AB}	g_{AB}
water		1	0	1
EO	polar	2	0[a]	1[a]
	nopolar	3	5.086[a]	8[a]
PO	polar	4	0[b]	1[b]
	nopolar	5	11.5[6]	60[b]

	$kT\chi_{BB'}$			
state no.	2	3	4	5
1	0.6508[a]	5.568[a]	1.7[b]	8.5[b]
2		1.266[a]	1.8[c]	3.0[c]
3			0.5[c]	−2.0[c]
4				1.4[b]

[a] From the fit to the experimental data of the binary PEO/water phase diagram.[17,24] [b] From the fit to the experimental data of the binary PPO/water phase diagram.[18] [c] From the fit to the experimental data of the ternary PEO/PPO/water phase diagram.[6]

have been determined from an independent analysis of the experimental data for the corresponding homopolymers[17,18,24] and are displayed in Table 1. Including this partition function in the overall partition function for the system, we exponentiate the expression given by eq 3 and include the new terms in an effective potential $\omega_p^{\text{eff}}[\mathbf{r}_p(t')]$, given by

$$\omega_p^{\text{eff}}(\mathbf{r}) = -\ln\{\sum_\alpha g_{p\alpha} \exp[-\beta E_{p\alpha} - \omega_{p\alpha}(\mathbf{r})]\} \quad (4)$$

Note that in so doing we have enlarged the set of conjugate fields to include every polymer component in its particular internal state, $\omega_{p\alpha}(\mathbf{r})$. Although the internal degrees of freedom of the polymer chains are independent of their spatial arrangement, they are imbedded in an inhomogeneous mean field which represents the average local arrangement of all the chains. The resulting effective mean field, given by eq 4, represents the statistically weighted thermal distribution of the internal states in an "external" mean field, $\omega_{p\alpha}(\mathbf{r})$, which reflects the local arrangement of the molecules. The modified diffusion equation for $Q_p(\mathbf{r}, t|\mathbf{r}_0)$ then follows the standard form

$$\frac{\partial}{\partial t}Q_p(\mathbf{r}, t|\mathbf{r}_0) = \frac{b^2}{6}\nabla^2 Q_p(\mathbf{r}, t|\mathbf{r}_0) - \omega_p^{\text{eff}}(\mathbf{r})Q_p(\mathbf{r}, t|\mathbf{r}_0) \quad (5)$$

and the introduction of the mean-field approximation by the evaluation of the functional integral by the method of steepest descents at the saddle point gives

$$\rho_s(\mathbf{r}) = \frac{N_s}{Q_s}\exp[-\omega_s(\mathbf{r})] \quad (6)$$

$$\rho_{p\alpha}(\mathbf{r}) = P_{p\alpha}(\mathbf{r})\rho_p(\mathbf{r}) \quad (7)$$

$$P_{p\alpha}(\mathbf{r}) = \frac{g_{p\alpha} \exp[-\beta E_{p\alpha} - \omega_{p\alpha}(\mathbf{r})]}{\sum_\alpha g_{p\alpha} \exp[-\beta E_{p\alpha} - \omega_{p\alpha}(\mathbf{r})]} \quad (8)$$

where $\rho_s(\mathbf{r})$ and $\rho_p(\mathbf{r})$ are the solvent and polymer densities, $P_{p\alpha}$ is the probability of a polymer segment in the internal state α, and eqs 7 and 8 are obtained by the application of the chain rule in the differentiations with respect to the polymer densities.

The expressions for the homopolymer densities in terms of the distribution functions are the same as in earlier work[15]

$$\rho_p(\mathbf{r}) = \frac{N_p}{Q_p}\int_0^{Z_p} dt q_p(\mathbf{r}, t)q_p(\mathbf{r}, Z_p - t) \quad (9)$$

$$Q_p = \int d\mathbf{r} \int d\mathbf{r}_0 Q_p(\mathbf{r}, Z_p|\mathbf{r}_0) \quad (10)$$

$$q_p(\mathbf{r}, t) = \int d\mathbf{r}_0 Q_p(\mathbf{r}, t|\mathbf{r}_0) \quad (11)$$

and the expressions for the mean fields are given by

$$\omega_s(\mathbf{r}) = \frac{\delta\beta U_{\text{pot}}(\{\rho\})}{\delta\rho_s(\mathbf{r})} + \eta(\mathbf{r}) \quad (12)$$

$$\omega_{p\alpha}(\mathbf{r}) = \frac{\delta\beta U_{\text{pot}}(\{\rho\})}{\delta\rho_{p\alpha}(\mathbf{r})} + \eta(\mathbf{r}) \quad (13)$$

where $U_{\text{pot}}(\{\rho\})$ is the potential energy of the system and the function $\eta(\mathbf{r})$ is chosen to satisfy the incompressibility conditions. Under the assumption of short-range interactions, the interaction potential $U_{\text{pot}}(\{\rho\})$ has the form

$$U_{\text{pot}}(\{\rho\}) = \int d\mathbf{r}\left\{\sum_{k\alpha} U_{s,k\alpha}\rho_s(\mathbf{r})\rho_{k\alpha}(\mathbf{r}) + \frac{1}{2}\sum_{k\alpha,k'\alpha'} U_{k\alpha,k'\alpha'}\rho_{k\alpha}(\mathbf{r})\rho_{k'\alpha'}(\mathbf{r})\right\} \quad (14)$$

where $U_{s,k\alpha}$ is the contact interaction energy between solvent molecule and monomers and $U_{k\alpha,k'\alpha'}$ is the contact interaction energy between different monomers. The interaction parameters of the various polymer components in their different internal states have also been determined from experimental data of homopolymers in solution and are given in Table 1.

For our system of solvent (water) molecules and PEO−PPO−PEO (A_1−B−A_2) triblock copolymers contained in a volume V, the free energy of the system in the mean-field approximation is given by

$$\frac{F}{k_B T\rho_{0s}V} = \frac{1}{V}\int d\mathbf{r}\left\{\sum_{k\alpha}\chi_{s,k\alpha}\phi_s(\mathbf{r})\phi_{k\alpha}(\mathbf{r}) + \frac{1}{2}\sum_{k\alpha,k'\alpha'}\chi_{k\alpha,k'\alpha'}\phi_{k\alpha}(\mathbf{r})\phi_{k'\alpha'}(\mathbf{r}) + \phi_s(\mathbf{r})\ln\phi_s(\mathbf{r}) - \sum_{k\alpha}\frac{\rho_{0k}}{\rho_{0s}}\omega_{k\alpha}(\mathbf{r})\phi_{k\alpha}(\mathbf{r})\right\} + \frac{\bar{\phi}_c}{\tau_c}\ln\left(\frac{\bar{\phi}_c}{Q_c}\right) \quad (15)$$

where we have introduced the local volume fractions $\phi_s(\mathbf{r}) = \rho_s(\mathbf{r})/\rho_{0s}$, $\phi_{cp}(\mathbf{r}) = \rho_{cp}(\mathbf{r})/\rho_{0p}$, etc., and the solvent density, ρ_{0s}, is taken as the reference density in defining the Flory−Huggins parameters

$$\chi_{k\alpha,k'\alpha'} = \beta U_{k\alpha,k'\alpha'}\rho_{0k}\rho_{0k'}/\rho_{0s} \quad (16)$$

The effective degrees of polymerization τ_{cp} are $\tau_{cp} = (\rho_{0s}/\rho_{0p})Z_{cp}$, and $\tau_c = \tau_{cA_1} + \tau_{cB} + \tau_{cA_2}$. The *overall* volume fraction of copolymer is denoted by $\bar{\phi}_c$. For the triblock copolymers the chain conformation contribution to the partition function, Q_c, is given by[15]

$$Q_c = \int d\mathbf{r}_1 d\mathbf{r}_2 d\mathbf{r}_3 d\mathbf{r}_4 Q_{A_1}(\mathbf{r}_1, Z_{A_1}|\mathbf{r}_2) Q_B(\mathbf{r}_2, Z_B|\mathbf{r}_3) Q_{A_2}(\mathbf{r}_3, Z_{A_2}|\mathbf{r}_4) \quad (17)$$

where the propagators $Q_{cp}(\mathbf{r}, t|\mathbf{r}')$ individually satisfy the biased diffusion equation, with the initial condition $Q_{cp}(\mathbf{r}, 0|\mathbf{r}') = \delta(\mathbf{r} - \mathbf{r}')$. The volume fractions (densities) of the different monomers are given by eqs 9−11, normalized by the integrals of the appropriate Q_{cp}. The computational algorithm used for solving the self-consistent mean-field equations with the incompressibility constraint has been described earlier.[25]

B. Lattice Description. We now describe the lattice model for multicomponent mixtures of copolymers with internal degrees of freedom occurring in heterogeneous systems.[18] The theory is based on the lattice theory by Scheutjens and Fleer[13] and the specific developments for describing micellization.[26,27] Here we provide a shorter account of the general theory adapted to the calculations of the ordered block copolymer phases. The presentation is slightly reformulated to facilitate a comparison with the continuum description.

The space between the two reflective surfaces (planar geometry) and the space within the reflective curved boundaries (cylindrical or spherical geometry) is divided into M layers. The parallel, or concentrical layers starting from the center, are numbered $i = 1, 2, ..., M$, each layer containing L_i lattice sites; the number of sites increases with i and is not necessarily an integer. Since within each layer the Bragg−Williams approximation of random mixing is applied, all the lattice sites in a layer are equivalent. The number of nearest-neighbor sites, z, the fraction of these sites in the same layer, λ_{ii}, and the fraction of these in adjacent layers $i' = i \pm 1$, $\lambda_{ii'}$, are dependent on the lattice topology. In the case of a planar hexagonal lattice as used here, $z = 12$ and $\lambda_{ii} = 0.5$. We consider the case in which each site is occupied by one solvent molecule or by one polymer segment. Since there are no nearest neighbors in nonadjacent layers, i.e., $\lambda_{ii'} = 0$ if $|i - i'| > 1$, and since the flux constraint implies $L_i\lambda_{ii'} = L_{i'}\lambda_{i'i}$, $i' = i \pm 1$, the λ matrix describing the lattice topology is fully determined.

The lattice is completely filled by a mixture of two components (polymer and solvent). There are n_x molecules of component x, each molecule consisting of τ_x segments. Since we are dealing with triblock copolymers, two types of polymer segments are involved. The segment types, which will be referred to as species, are generically labeled A, A', etc.

The various conformations of the polymer chains are distinguished in terms of the different ordering of their segments with respect to the layer numbers. A conformation c of component x is described by an ordered set of layer numbers $k(x,s,c)$; $s = 1, ..., \tau_x$ where $k(x,s,c)$ is the number of the layer in which the segment of rank s (the sth segment in the chain) of the component x in the conformation c is located. The degeneration of a component x in conformation c, neglecting self-exclusion, becomes $\omega_{xc} z^{\tau(x)-1}$ where

$$\omega_{xc} = L_{k(xc,1)} \prod_{s=2}^{\tau_x} \lambda_{k(x,c,s-1),k(x,c,s)} \quad (18)$$

and $L_{k(x,c,1)}$ indicates the number of possibilities for the position of the first segment, consistent with conformation c, and the product of λ elements representing the probability of the remaining $s - 1$ segments likewise being consistent with conformation c.

The derivation of the internal state and of the segment distributions starts with the partition function of the model system. After replacement of the partition function with its largest term, the Helmholtz free energy of the system, relative to a reference state involving its separate amorphous components, may be expressed as[18]

$$\beta(A - A^*) = \beta(A_{int} - A^*_{int}) - \ln \frac{\Omega}{\Omega^*} + \beta(U - U^*) \quad (19)$$

where $\beta = (kT)^{-1}$, k being Boltzmann's constant and T the absolute temperature. The first term denotes the contribution arising from the internal degrees of freedom, the second term is the mixing entropy, and the third is the mixing energy.

Each state of a species is characterized by an energy term, E_{AB}, and a degeneration factor, g_{AB}, where in both cases A denotes the species and B the state of species A. The total internal free energy arising from the internal states becomes

$$\beta A_{int} = \sum_i \sum_A n_{Ai} \sum_B P_{ABi} \left[\beta E_{AB} + \ln \frac{P_{ABi}}{g_{AB}} \right] \quad (20)$$

where $\sum_i$ denotes the sum over layers, $\sum_A$ the sum over species (segment types), and $\sum_B$ the sum over the states of species A, n_{Ai} is the number of sites in layer i occupied by segments of type A, and P_{ABi} is the fraction of species A in layer i which is in state B. There are three contributions to the internal free energy, namely, E_{AB}, which is the internal energy of state B of species A; $-kT$ ln g_{AB}, where g_{AB} is the degeneration factor of state B of species A; and kT ln P_{ABi}, an entropy term arising from the mixing of the states. In the case of EO (or PO), E_{AB} and g_{AB} describe the equilibrium between the polar and nonpolar states of EO (PO). Since the nonpolar state has a higher internal energy and greater degeneracy, $E_{EO,nonpolar} > E_{EO,polar}$ and $g_{EO,nonpolar} > g_{EO,polar}$. Finally, A^*_{int} may be set to zero by a suitable choice of the reference state.

The mixing entropy arises from the difference between the configurational degeneracy of the system and of the reference state. When self-exclusion at a mean-field level is taken into account, and the contributions of all the conformations of all the components are included, the mixing entropy of the system can be expressed as[18]

$$\ln \frac{\Omega}{\Omega^*} = -\sum_x \sum_c n_{xc} \ln \frac{n_{xc}\tau_x}{\omega_{xc}} \quad (21)$$

where n_{xc} denotes the number of chains of component x in conformation c and where ω_{xc}, which is related to the degeneracy of component x in conformation c, is given by eq 18.

Finally, within the mean-field approximation the interaction energy is given by[18]

$$\beta U = \frac{1}{2} \sum_{i=1}^{M} L_i \sum_A \sum_{A'} \sum_B \sum_{B'} \phi_{Ai} P_{ABi} \chi_{BB'} \langle P_{A'B'i} \phi_{A'i} \rangle \quad (22)$$

when $\langle x_i \rangle \equiv \sum_{i'=1}^{i'=M} \lambda_{ii'} x_{i'}$ and ϕ_{Ai} is the volume fraction of species A in layer i. In the case of nearest-neighbor interactions only, the sum over i' in the definition of $\langle x_i \rangle$ contains at most three terms. In eq 22, χ_{BB} denotes

the Flory−Huggins interaction parameter,[14] traditionally defined as $\chi_{BB'} = \beta z[\epsilon_{BB'} - (\epsilon_{BB} + \epsilon_{B'B'})/2]$, where $\epsilon_{BB'}$ is the interaction energy on a site-volume basis between species A in state B and species A' in state B'. In expressions such as eq 18, the state summation variable B is always associated with the species summation variable A, B' summed with A', etc. The reference interaction energy U^* becomes nonzero in the presence of two different species in the separated-polymer reference system as given by eq A.5.2 in ref 18. Since we have a periodic system, we apply reflective boundary conditions, i.e., $\phi_{A,i=M} = \phi_{A,i=M+1}$ and also $\phi_{A,i=1} = \phi_{A,i=0}$ for the planar geometry.

The state equilibrium distribution $\{P_{ABi}\}$ and the conformational equilibrium distribution $\{n_{xc}\}$ are obtained by selecting the most important term in the partition function which fulfills the constraints $\sum_B P_{ABi} = 1$ and $\sum_x \sum_c n_{xc}\tau_{xci} = L_i$, where τ_{xci} is the nubmer of segments in component x and in conformation c which are in layers i. In the following we will give the relevant expressions of the state equilibrium distribution $\{P_{ABi}\}$ and of the segment equilibrium distribution $\{n_{xsi}\}$, the latter being uniquely determined by the conformational equilibrium distribution $\{n_{xc}\}$.

Thus, $\{n_{xsi}\}$, the number of sites in layer i occupied by segments of rank s belonging to component x, is obtained by generating all possible chain configurations with appropriate weights. By a matrix representation, it can be expressed as[18]

$$n_{xsi} = C_x\{\Delta_i^T[\prod_{s'=\tau_x}^{s+1}(\mathbf{W}^{t(x,s')})^T]\mathbf{s}\}\{\Delta_i^T\cdot[\prod_{s'=2}^{s}\mathbf{W}^{t(x,s')}]\cdot\mathbf{p}(x, 1)\} \tag{23}$$

where C_x is a normalization factor related to the amount of component x (canonical ensemble which is used for the calculations of the ordered phases) or the bulk volume fraction of component x with which the system is in equilibrium (grand canonical ensemble which is used for the micelle calculations), $\mathbf{W}^{t(x,s)}$ a tridiagonal matrix comprising elements that contain factors describing the lattice topology and the factors containing the potential for segments of rank s belonging to component x, and $\mathbf{p}(x, 1)$ a vector describing the distribution of the first segment of component x among the layers, Δ and $\mathbf{s}$ being elementary column vectors. The potential u_{Ai} for segment s of the type A in layer i entering $\mathbf{W}$ is given by

$$\beta u_{Ai} = -\ln\{\sum_B P_{AB}^b \exp[-\beta u_{ABi}]\} \tag{24}$$

In the grand canonical ensemble, the weighting factor P_{AB}^b of state B of species A is given by

$$P_{AB}^b = \frac{g_{AB}\exp[-\beta E_{AB} - \sum_{A'}\sum_{B'}\chi_{BB'}P_{A'B'}^b\phi_{A'}^b]}{\sum_B g_{AB}\exp[-\beta E_{AB} - \sum_{A'}\sum_{B'}\chi_{BB'}P_{A'B'}^b\phi_{A'}^b]} \tag{25}$$

and the state specific potential u_{ABi} by

$$\beta u_{ABi} = \beta u_i' + \sum_{A'}\sum_{B'}\chi_{BB'}(\langle P_{A'B'i}\phi_{A'i}\rangle - P_{A'B'}^b\phi_{A'}^b) \tag{26}$$

The corresponding expressions in the canonical ensemble are formally obtained by setting $\phi_{A'}^b = 0$. The species-independent potential u_i' in eq 26 ensures that the space is completely filled at layer i and is related to the lateral pressure in the continuous description. The other term involves the nearest-neighbor interactions and consists of the mixing energy for species A in state B in layer i being diminished by the corresponding mixing energy in bulk. Again $\phi_{A'}^b = 0$ in the canonical ensemble. The state distribution P_{ABi} can be expressed in terms of the state potential and weights P_{AB}^b according to

$$P_{ABi} = \frac{P_{AB}^b \exp[-\beta u_{ABi}]}{\sum_B P_{AB}^b \exp[-\beta u_{ABi}]} \tag{27}$$

Finally, the species volume fraction ϕ_{Ai} needed in eq 26 is simply related to n_{xsi} according to

$$\phi_{Ai} = \frac{1}{L_i}\sum_x\sum_{s=1}^{\tau_x}\delta_{A,t(x,s)}n_{xsi} \tag{28}$$

where L_i is the number of sites in layer i. The Kronecker δ selects only segments of rank s of component x if they are of type A. Since u_{ABi} is needed to obtain n_{xsi} through eqs 23 and 24 and u_{ABi} depends itself on n_{xsi} through eqs 26−28, eqs 23 and 24 and 26−28 have to be solved self-consistently. For the purpose of facilitating comparisons between the continuum and lattice descriptions of the self-consistent mean-field theory, Table 2 summarizes some equivalent notations used in both versions of the theory.

Table 2. Equivalence of Notation for Continuum and Lattice descriptions of Self-Consistent Mean-Field Theory

continuum	lattice
$g_{p\alpha}$	g_{AB}
$E_{p\alpha}$	E_{AB}
$\omega_p^{eff}(\mathbf{r})$	βu_{Ai}
$\omega_{p\alpha}(\mathbf{r})$	βu_{ABi}
$P_{p\alpha}(\mathbf{r})$	P_{ABi}
	$P_{AB}^b = g_{AB}\exp(-\beta E_{AB})$ (fixed amount)
$q_p(\mathbf{r}, t)$	$\Delta_i^T\cdot[\prod_{s'=2}^{s}\mathbf{W}^{t(x,s')}]\cdot\mathbf{p}(x, 1)$
eq 9	eq 23 with additional summation over s
eq 4	eq 24
eq 8	eq 27

C. Micelle Model within the Lattice Description. At low polymer volume fraction, a solution of polymer micelles may be formed by the block copolymers. The calculation of the critical micellar concentration, the lowest concentration at a given temperature where micelles are formed, is carried out as described earlier.[22]

Briefly, the micellar solution is (hypothetically) divided into spherical subsystems (cells), each of which contains one micelle and its accompanying solution. The volume of the subsystem V_s is simply the inverse micellar number density. The excess free energy A_s of a subsystem contains two parts: A^σ, which is the free energy associated with the formation of a micelle fixed in space in contact with the bulk solution, and the mixing entropy, as given by

$$\beta A_s = \beta A^\sigma + \ln\frac{V_m}{V_s} \tag{29}$$

where V_m is the volume of the micelle. A necessary requirement for stable micelles at equilibrium is that

the positive A^σ be balanced by the favorable mixing entropy of the micelle, implying that $A_s = 0$. Given that the equilibrium state and the segment distributions are determined, A^σ is obtained from

$$A^\sigma = (A - A^*) - \sum_x n_x(\mu_x - \mu_x^*) \tag{30}$$

where $A - A^*$ is given by eq 19 and $\mu_x - \mu_x^*$ denotes the difference between the chemical potential of component x in bulk and in the reference state given by eq 15 in ref 7.

An important quantity is the excess number of segments of component x in the subsystem, defined as

$$\Gamma_x = \sum_{i=1}^{M} L_i[(\sum_{s=1}^{\tau_x} \phi_{xsi}) - \phi_x^b] \tag{31}$$

where $\phi_{xsi} = n_{xsi}/L_i$, and the excess number of polymer molecules is the aggregation number of the micelle, $N_{agg} = \Gamma_{polymer}/\tau_{polymer}$. Given $\Gamma_{polymer}$, the micellar volume is approximated by

$$V_m = \frac{\Gamma_{polymer}}{\phi_{polymer,i=1} - \phi_{polymer}^b} \tag{32}$$

where $\phi_{polymer,i=1}$ represents the polymer volume fraction in the core (any layer within the core would do since $\phi_{polymer}$ is nearly constant in the core). Finally, the total volume fraction of component x in the subsystem, $\bar{\phi}_x$ (equal to the stochiometric concentration of x in the micellar solution), is the sum of the excess and bulk volume fractions according to

$$\bar{\phi}_x = \frac{\Gamma_x}{V_s} + \phi_x^b \tag{33}$$

Thus, on the basis of a selected bulk composition and the equilibrium state and segment distributions, the excess free energy of the subsystem is obtained from eq 30. Equation 31 is then used to compute the amount of excess polymer, eq 32 to obtain the micellar volume, and eq 29 to obtain the volume of the subsystem, whereas the total composition is finally obtained from eq 33. Any change in the bulk composition leads to a change in the total concentration, with concomitant changes in the micellar structures, or possibly to no micelles formed at all. The lowest total polymer concentration at which stable micelles exist (which requires $A^\sigma > 0$ and $\partial A^\sigma/\partial N_{agg} < 0$) will be referred to as the critical micelle concentration (cmc).

III. Ordered Phases

In this section we present the calculated phase diagrams of EO−PO−EO triblock copolymers in water, as a function of polymer volume fraction, $\bar{\phi}_c$, and temperature. From the Pluronic grid (Figure 2) we chose a triplet series (P103, P104, P105) to study the effect of changing the weight percent of poly(ethylene oxide) while keeping the molecular weight of poly(propylene oxide) constant, and one system (P94) to study the effect of changing the molecular weight of the poly(propylene oxide) while keeping the weight percent of poly(ethylene oxide) constant. It has been shown experimentally, using ^{2}H NMR, SAXS, and polarizing microscopy, that cubic, hexagonal, and lamellar lyotropic liquid crystalline phases may self-assemble, depending on the polymer molecular weight, chemical composition, temperature, and concentration. In addition, micellization and cloud point formation can take place, depending on the specifics of these variables. Here we are mainly concerned with identifying the trends encountered by changing these factors, and in discovering the underlying principles, utilizing the theoretical models, which are responsible for the trends.

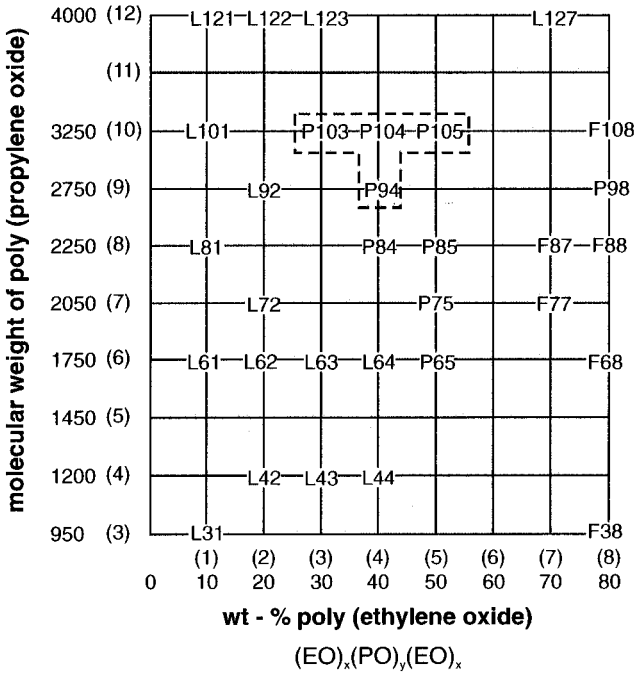

Figure 2. Grid showing weight percent poly(ethylene oxide) vs molecular weight of poly(propylene oxide) (so-called Pluronic grid) for EO−PO−EO triblock copolymers, with those copolymers discussed in this paper surrounded by dashed lines. Adapted from Schmolka.[36]

We first recall that the formation of ordered phases in block copolymer melts (without a selective solvent) has been studied in great detail, both experimentally[28−33] and theoretically.[10,15,16,34,35] Most of the work has centered around diblocks instead of triblocks, but the physical principles of mesophase formation are the same in both cases. For diblocks, the incompatible A and B blocks ($\chi_{AB} > 0$) segregate to reduce the enthalpy of mixing, at the expense of reducing the entropy (thereby increasing the free energy) because the necessity of filling the ordered domains uniformly requires chain stretching. The equilibrium domain size and shape can be determined by balancing the entropic changes due to chain stretching with the free energy of formation of the domain boundaries to give the lowest overall free energy. The minimum block sizes (both relative and absolute) and interaction parameters for the formation of the different ordered phases from the disordered melt can also be determined in this way.

The physical picture described above can be translated into simple scaling laws, complemented by the self-consistent mean-field calculations. Near the order−disorder phase boundary, however, fluctuations must be included in the mean-field description to give meaningful description of the self-assembled structures. With a strongly selective solvent to the system, the simple scaling picture becomes less general due to the number of limiting cases and complementary mean-field calculations are again important for obtaining insight into the behavior of the system.

A. Phase Diagrams. The determination of the PEO−PPO−PEO block copolymer−water phase diagrams containing up to five ordered phases and one disordered phase was carried out in the same way for both the continuous and discrete (lattice) models. That is, for each temperature and overall composition, the free energies of six phases were calculated, and moreover, for each ordered phase the domain spacing was also optimized. We have here simplified the procedure by disregarding the two-phase regions around the one-phase boundaries (our main aim was to examine the approximate locations of the one-phase regions and to study their shift with composition as well as the structure of the repetitive domains—the two-phase regions may be obtained by the usual double-tangent constructions). This allowed us to find the phase boundaries by considering the crossings of the free energy curves of the phases. Finally, the large contribution to the free energy from the internal degrees of freedom makes $\beta(A - A^*)$ almost linearly dependent on $\bar{\phi}_c$. By considering $\beta A_{mod} \equiv \beta(A - A_{hom})$, where A_{hom} is the corresponding free energy of the homogeneous (disordered) phase with the same composition, the crossings of the free energy curves were easily determined. The phase boundary for micelle formation was calculated only with the discrete lattice model and is given only for Pluronic P94. Since the calculation of the phase boundaries of the ordered phases gave similar results for both the continuum and discrete models, we felt that using the micellization model developed earlier was sufficient for this purpose. Finally, to obtain real length units, we have used $b = 4$ Å as the Kuhn length and also 4 Å as the length of a lattice cell. The latter assignment has been shown to given good agreement with various experimental data.[7]

We now look in detail at the P94−water binary-phase diagram (composition vs temperature). Referring to the experimental work of Zhang and Khan and focusing on a temperature around $T = 35$ °C, they found that the phases with increasing polymer concentration (weight percent) show the same ordered symmetries as for block copolymers with variable composition but without a selective solvent, beginning at low polymer concentrations with an isotropic water-rich phase followed by a cubic phase, continuing with hexagonal and lamellar phases, and ending with an isotropic polymer-rich phase. The two-phase regions shown in the experimental diagram will not be discussed here, and we will concentrate on the boundaries between these phases. The experimental phase diagram of Zhang and Khan is reproduced in Figure 3.

The theoretically calculated phase diagram is shown in Figure 4. The solid lines show the results of the calculations based on the continuum model, and the dashed lines show the results for the lattice model. The region of a disordered solution of micelles is represented by the hatched area. The precise location of the boundary between this region and the ordered cubic phase (I1) cannot be determined unambiguously, since the individual micelle description becomes less reliable at larger polymer volume fractions, where the micelles begin to overlap. As the polymer volume fraction is further increased, there are successive transitions from the ordered cubic phase to the hexagonal phase (H1), lamellar phase (L_α), inverse hexagonal phase (H2), inverse ordered cubic phase (I2), and a disordered polymer-rich solution (L2). There are many similarities to the experimental phase diagram but also some differences. At increasing temperature, the lattice calculation shows a two-phase region at temperatures lower than that observed in the continuum model and in the experiments. There is also a shift in the location of the phase boundary between the isotropic and cubic phases as predicted by the continuum model and the lattice model. The free energy of the solution with disordered micelles however is lower than that of the disordered isotropic phase without micelles, and the boundary between the disordered micelles and the ordered cubic domain is shifted to higher polymer concentrations than indicated by the isotropic solution model (cf. hatched area and dashed line). The transition between structures as predicted on the basis of the lattice model is more realistic in this case and the theoretically predicted transition from disordered to ordered micelles also takes place close to the region shown on the experimental phase diagram.

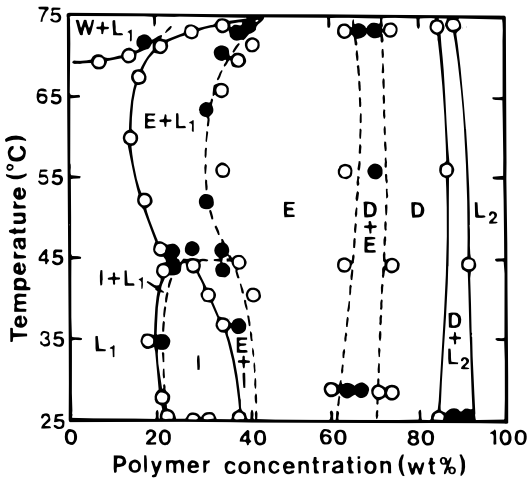

Figure 3. Binary phase diagram (composition vs temperature) for the system P94 ($(EO)_{21}(PO)_{47}(EO)_{21}$−water (After Figure 2 of ref 2, with permission): L_1, L_2, and W, isotropic solution phases; E, hexagonal; D, lamellar; I, cubic liquid crystalline phases; D + E, E + I, etc., two-phase regions. Solid lines are accurate to ±1%, and broken border lines are less accurate. The filled and empty circles correspond to the experimental point in the different phases.

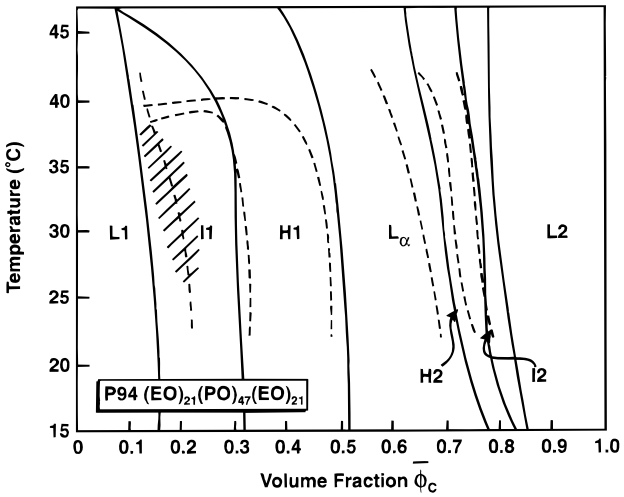

Figure 4. Calculated phase diagram for Pluronic P94 $(EO)_{21}$-$(PO)_{47}(EO)_{21}$. The solid and dashed lines are calculated from the continuum and lattice descriptions, respectively. The hatched area shows the region with a disordered solution of micelles. L1 refers to a disordered polymer poor solution, I1 the ordered cubic phase, H1 the hexagonal phase, L_α the lamellar phase, H2 the inverse hexagonal phase, I2 the inverse cubic phase, and L2 a disordered polymer-rich solution.

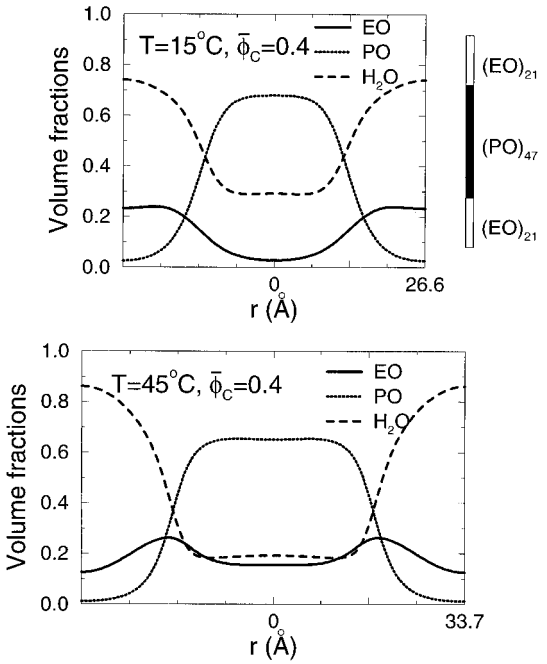

Figure 5. Volume fractions of monomeric components for P94, hexagonal phase (H1), including water, for low (T = 15 °C) and high (T = 45 °C) temperature points on the phase diagram shown in Figure 3, with an overall copolymer volume fraction $\bar{\phi}_c = 0.4$.

Other differences between the theoretical and experimental diagrams should be attributed to the idealizations inherent in our models as well as to sample polydispersities and the differences in the copolymer volume fractions used here as compared to the concentration by weight percent. Also, the theoretical diagram predicts inverse phases at higher polymer concentrations. However, the free energy differences between the different phases are very small in this case and it is not surprising that the inverse phases, if they exist, are not easily observed in the experiments.

B. Density Profiles. Besides the phase boundaries, other important features predicted from the theoretical model are the density profiles. The density profiles for the hexagonal phase (H1) are shown in Figure 5 for P94, based on the continuum model. We have chosen two temperatures T = 15 and 45 °C to demonstrate the changes arising from the decrease of the solubility of the EO and PO in water as the temperature is increased. At the lower temperature the cylindrical domain shows a high concentration of PO in the middle, with a corresponding low concentration of EO and a tendency for the water to stay in the EO domain because of the hydrophilic behavior of the ethylene oxide at this temperature. At the higher temperature there are considerable changes in the density profiles. As EO becomes more hydrophobic, it tries to withdraw into the middle of the domain to reduce its contact with water. However, EO and PO are not fully compatible, hence the EO density profile develops a maximum around the edges of the PO region as it tries to compromise its position between the PO filled middle and the hydrophilic outside of the domain. The water content in the PO-rich middle of the domain as well as in the ethylene oxide-rich outside regions is also smaller than at the lower temperature.

Another important feature is that the domain spacing is increased at the higher temperature, indicating that there is a smaller interfacial area for the molecules at the higher temperature, consistent with the increased hydrophobicity of the EO and PO blocks. The density profiles are displayed in terms of gray-scale images in Figure 6, with the spatial scale also indicated. At the lower temperature there is a clear distinction between the hexagonally ordered PO domains, the EO in the matrix between the hexagonally ordered domains, and the high water content accompanying the EO matrix. At the higher temperature there is a substantial increase in the domain spacing (note that the spatial scale is same on the gray-scale images for the two temperatures) corresponding to the smaller interfacial area per molecule. The secondary ringlike structure for EO domains is clearly visible at the higher temperature. The size is larger for both the EO and PO regions, and there is still a tendency for the water to localize between the PO domains.

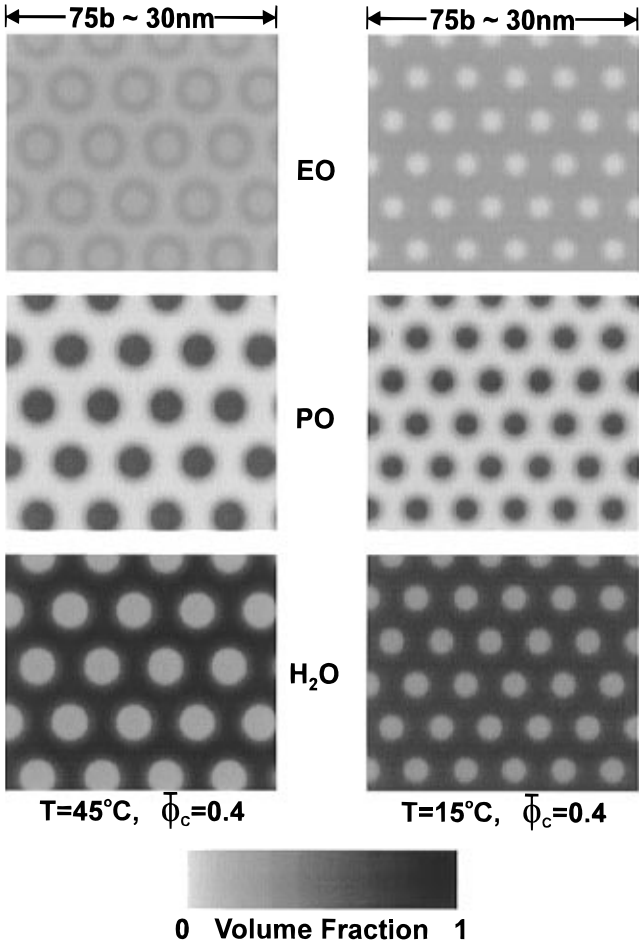

Figure 6. Gray-scale images corresponding to the volume fractions for P94, hexagonal phase (H1) (shown in Figure 5), at T = 15 °C and T = 45 °C, with an overall volume fraction of copolymer $\bar{\phi}_c = 0.4$.

For the lamellar phase L_α, the low-temperature profiles (Figure 7) show the PO domains having a strong maximum and the EO domains filled to a high level with water. For the higher temperature (Figure 7), the EO blocks again try to separate from the water by penetrating and broadening the PO region and give rise to secondary maxima at the edges of PO domain. The domain size is increased at the higher temperature but to a lesser extent than for the hexagonal domains because in this case there is less water in the system. The gray-scale images for the volume fractions in the different domains are shown in Figure 8 for the two temperatures.

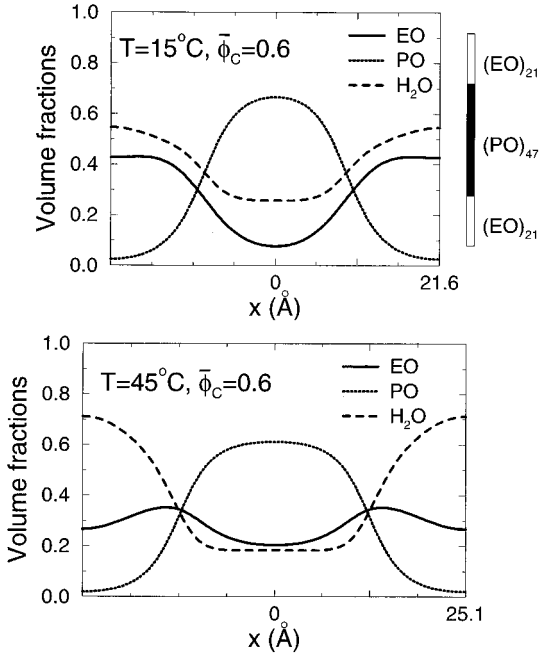

Figure 7. Volume fractions of monomeric components for P94, lamellar phase (L_α), including water, for low (T = 15 °C) and high (T = 45 °C) temperature points on the phase diagram shown in Figure 3, with an overall copolymer volume fraction $\bar{\phi}_c = 0.6$.

We now consider the inverse hexagonal phase (H2). In this case, the low-temperature phase (Figure 9) shows a maximum for the EO content and an increase in the water concentration in the middle of the EO domains. At the higher temperature (Figure 9), there is more localization of the water into the middle of the domain, the EO domains develop secondary maxima, and the PO regions are broadened and have a larger EO content. The domain size in this case does not change very much between the higher and lower temperatures because the water content has been reduced to a lower concentration than for the other ordered phases. The gray-scale images in Figure 10 for two temperatures show the expected results, and the ring-like structure of the EO regions is barely visible.

The domain spacings of the ordered phases of Pluronic P94 at thermodynamic equilibrium are given in Figure 11. The increase of the domain size with increasing temperature is clearly seen, and we have previously attributed this effect of the thermodynamic tendency of increasing the separation between the water and the EO/PO segments. A slightly reformulated statement, which often is used in conjunction with the change in micellar structure, is that the dehydration of the EO segments at increasing temperature leads to a smaller head group area. Therefore, for the ordered phases a smaller interfacial area per EO segment necessarily leads to a larger domain spacing.

Also evident from Figure 11 is the reduction of the domain spacing at the phase transitions when the interface becomes less curved, with the smallest domain spacing occurring for the lamellar phase. As for block copolymers with organic solvents, phase transitions between morphologies take place in order to reduce the entropy loss due to chain stretching, and to decrease the interfacial area per unit volume, consistent with the enthalpic consequences of dilution with a selective solvent. Moreover, within a given ordered phase the domain spacing decreases or in some cases is nearly constant with increasing polymer concentration. Such

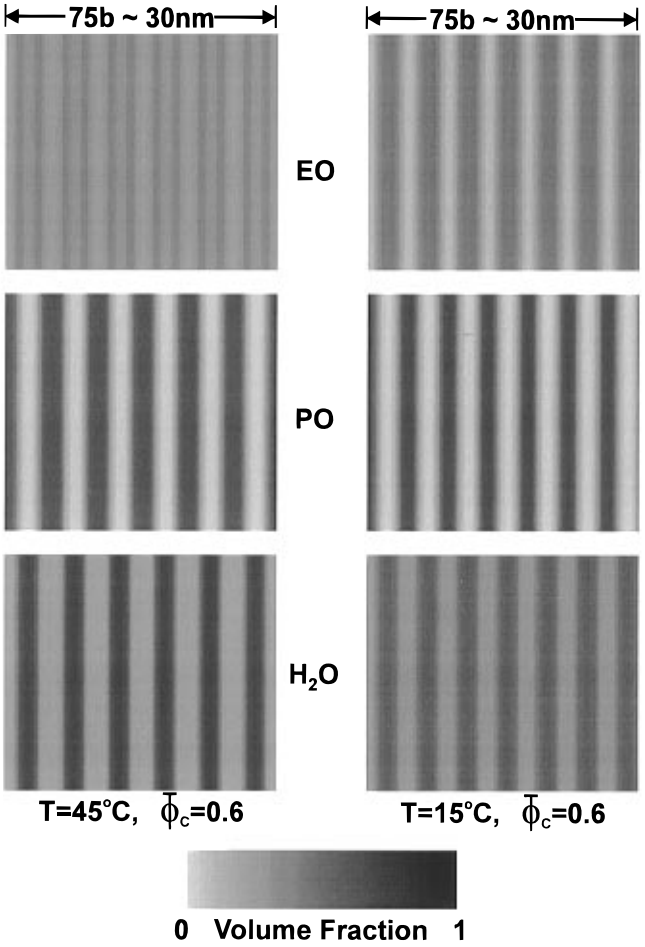

Figure 8. Gray-scale images corresponding to the volume fractions for P94, lamellar phase (L_α) (shown in Figure 7), at T = 15 °C and T = 45 °C, with an overall volume fraction of copolymer $\bar{\phi}_c = 0.6$.

a reduction accompanies the decrease in the amount of water per block copolymer forming the interface. The dependence of the spacing on the polymer concentration is particularly prominent at the higher temperature, and this hyperbolic-like behavior is expected where the incorporation of the water into the EO domains is small.

C. Junction Distributions. We now turn to the junction distribution functions and we concentrate on the P94 system. Since the propagators $Q_{cp}(\mathbf{r}, t|\mathbf{r}')$ contain all the information about the chain conformations, we can extract the junction distributions from the propagators. The solution of the mean-field equations gives a set of mean fields and equilibrium domain sizes, which can be used to obtain the propagators. It is then convenient to define two integrated propagators for the B block

$$q_{A_1B}(\mathbf{r}, t) = \int d\mathbf{r}_1 d\mathbf{r}_2 Q_B(\mathbf{r}, t|\mathbf{r}_1) Q_{A_1}(\mathbf{r}_1, Z_{A_1}|\mathbf{r}_2)$$

$$q_{A_2B}(\mathbf{r},t) = \int d\mathbf{r}_1 d\mathbf{r}_2 Q_B(\mathbf{r}, t|\mathbf{r}_1) Q_{A_2}(\mathbf{r}_1, Z_{A_2}|\mathbf{r}_2) \quad (34)$$

The probability distribution of the first joint is then given by

$$P_{\text{joint1}}(\mathbf{r}) = c q_{A_1B}(\mathbf{r}, 0) q_{A_2B}(\mathbf{r}, Z_B) \quad (35)$$

where c is a constant, which is chosen so that $P_{\text{joint1}}(\mathbf{r})$ is normalized to unity for a domain containing one interface. With the joint distribution $P_{\text{joint1}}(\mathbf{r})$ and the

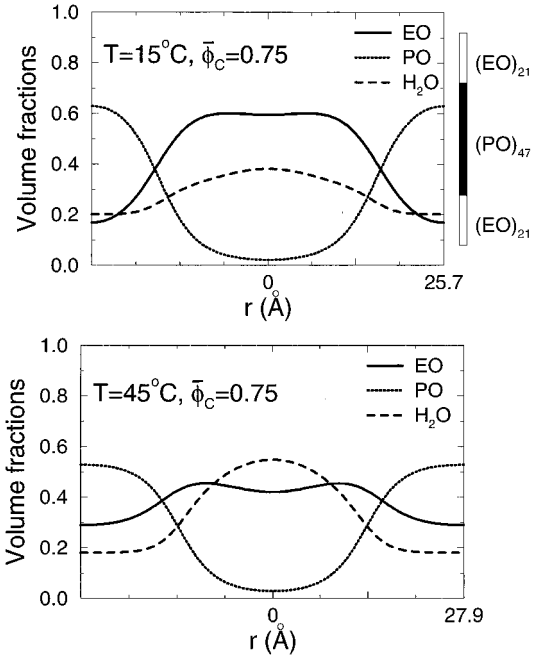

Figure 9. Volume fractions of monomeric components for P94, inverse hexagonal phase (H2), including water, for low (T = 15 °C) and high (T = 45 °C) temperature points on the phase diagram shown in Figure 3, with an overall copolymer volume fraction $\bar{\phi}_c$ = 0.75. Because the H2 region on the phase diagram is so narrow and shifts with temperature, the low-temperature (T = 15 °C) inverse hexagonal (H2) phase for $\bar{\phi}_c$ = 0.75 is metastable; however, we use this phase for comparison with the stable high-temperature (T = 45 °C) inverse hexagonal (H2) phase so that we can fix the overall copolymer volume fraction for the purpose of comparison.

propagators, we can determine the probability distribution of the second joint for those copolymer chains whose first joints are confined to a particular interface,

$$P_{\text{joint},2}(\mathbf{r}) = q_{A_2B}(\mathbf{r}, 0) \int d\mathbf{r}' Q_B(\mathbf{r}, Z_B|\mathbf{r}') P_{\text{joint1}}(\mathbf{r}') \quad (36)$$

In Figure 12 the calculated joint distribution functions are shown from T = 15 °C up to T = 45 °C. The probability distribution of the location of a joint across the lamellar domain, irrespective of the location of the other joint, is given by the solid curves, whereas its two components, where the second joint is restricted to $x > 0$ or $x < 0$, are given by the dotted and dashed curves, respectively. As can be seen, for lower temperatures, there is only a small difference in the two conditional distributions. However, at the higher temperature the conditional distributions clearly become more asymmetric and the overall joint distribution becomes more uniform across the domain. This is consistent with the earlier discussion relating to the increasing hydrophibicity of the EO blocks with increasing temperature. The greater amount of EO−PO mixing makes the overall joint distribution more uniform in the central region and the larger size of this region increases the probability of having both joints on the same side. For the hexagonal phase, a similar calculation (Figure 13) shows the overall distribution of the joints which again becomes more uniform with increasing temperature. Figures 14 and 15 show the mean-field potential experienced by the EO and PO segments in the lamellar and hexagonal phases, respectively. The crossover of the EO and PO potentials determines the location of the junctions of the triblocks. The sharpness of the crossover is deeper for the lower temperature than for the higher

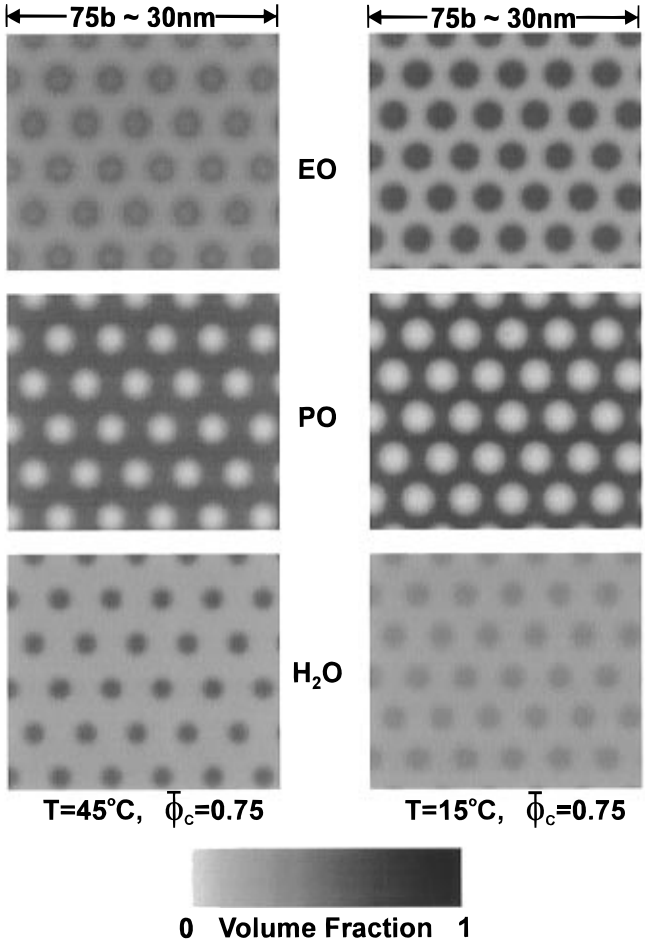

Figure 10. Gray-scale images corresponding to the volume fractions for P94, inverse hexagonal metastable phase (H2) (shown in Figure 9), at T = 15 °C and T = 45 °C, with an overall volume fraction of copolymer $\bar{\phi}_c$ = 0.75.

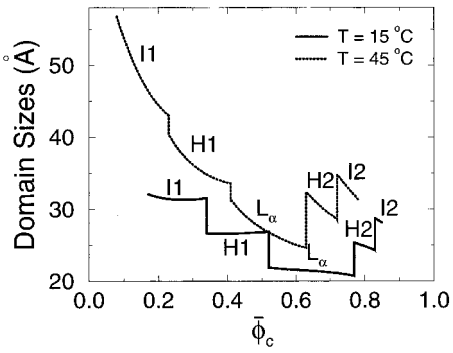

Figure 11. Equilibrium domain sizes corresponding to different overall volume fractions of copolymer P94, at T = 15 °C and T = 45 °C.

temperature, consistent with the temperature dependence of joint probability distributions shown earlier.

D. Shear Modulus. We will now discuss the expected changes in the shear modulus of the ordered phases as a function of the temperature using some of the results given above. In particular, we will consider the lamellar phase, and we believe that the most relevant parameters are (i) the volume fraction of EO segments between the different domains (in particular the volume fraction at the edges), (ii) the number of EO end blocks per unit area, and (iii) the conditional joint distribution functions.

First, we expect the yield under shear to appear in the water-rich region between the polymer regions.

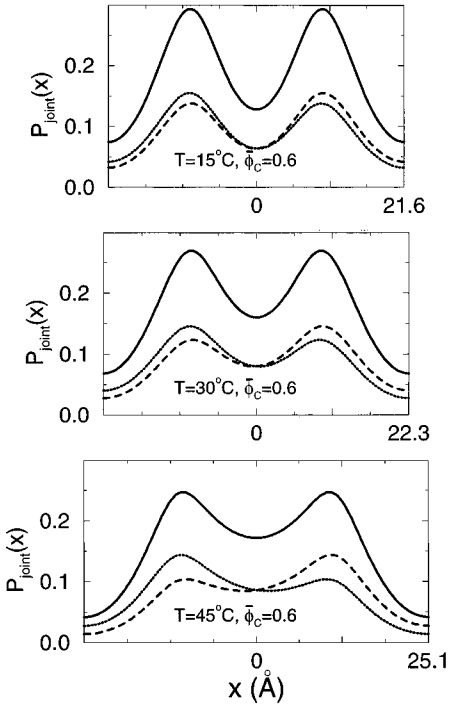

Figure 12. Equilibrium joint distribution functions for P94, lamellar phase (L_α), with an overall copolymer volume fraction $\bar{\phi}_c = 0.6$, for $T = 15$, 30, and 45 °C. The solid lines represent the probability distribution (normalized to unity for the domains containing one interface) for locating a joint anywhere across the lamellar domains. The dotted line is the joint distribution of the second joint given that the first joint is located in the left interfacial region. Finally, the dashed line is the joint distribution of the second joint given that the first joint is located in the right interfacial region. The sum of the dotted and dashed line gives the solid line.

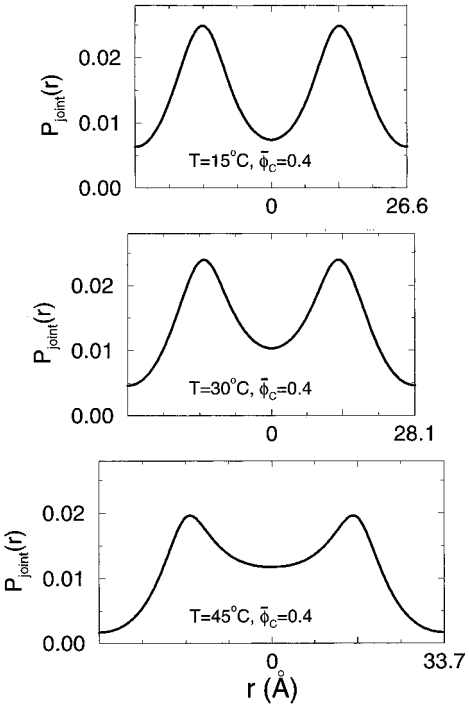

Figure 13. Equilibrium joint distribution function for P94, hexagonal phase (H1), for $T = 15$, 30, and 45 °C, with an overall copolymer volume fraction $\bar{\phi}_c = 0.4$. The solid lines represent the probability distributions (normalized to unity for the domains containing one interface) for locating a joint anywhere across a cut through the center of a cylindrical domain.

Although the fraction of PO blocks that traverse the PO regions is well below 50% at the higher temperature, the contour length of about 190 Å should be sufficient to form entangled loops in the approximately 20 Å wide PO region to keep the PO region together under shear.

Regarding the water-rich slip regions, the smaller EO fraction in these regions at the higher temperature results in less entanglements among EO end blocks from the different polymer domains and hence a smaller resistance to slip per chain. On the other hand, the domain spacing increases with temperature and the number of EO end blocks per unit interfacial area increases by about 16% from 10 to 45 °C. Thus, when the stress is considered per unit interfacial area, the two effects counterbalance. However, we believe that the reduction in the number of entanglements associated with the considerable decrease of the EO volume fraction from 0.42 to 0.27 is the dominating factor, and hence, we expect a reduction of the shear modulus with increasing temperature.

E. Change of Polymer Composition. We now briefly discuss the calculated phase diagrams for the other systems in the Pluronic grid. P104, in Figure 16, shows the same ordered phases as for P94. However, the liquid crystalline order persists over a wider concentration and temperature range. For P105, shown in Figure 17, the temperature range over which the liquid crystalline order persists is even larger and the phase boundaries have shifted to larger polymer volume fractions. The experimental diagram for P105 has been studied recently (Figure 2c in ref 5) and shows phase behavior very similar to the theoretical diagram. It should be noted that around 60 °C multiphase behavior

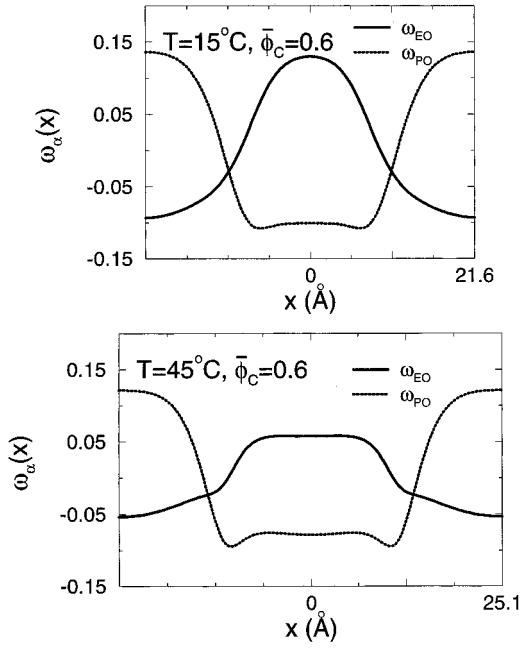

Figure 14. Mean-field potentials ω_{EO} and ω_{PO} for P94, lamellar phase (L_α), for $T = 15$ °C and $T = 45$ °C, with an overall copolymer volume fraction $\bar{\phi}_c = 0.6$.

is observed experimentally. We have not addressed this observation in the current set of calculations. For P103 (Figure 18), the temperature range over which liquid crystalline order persists is narrower and the phase boundaries are shifted to lower volume fractions than that for P104. Thus, an increased polymer length with constant EO/PO composition leads to more extended liquid crystalline ordered phases, which is expected since the tendency to segregate increases with polymer length. The shift of the boundaries with the number of

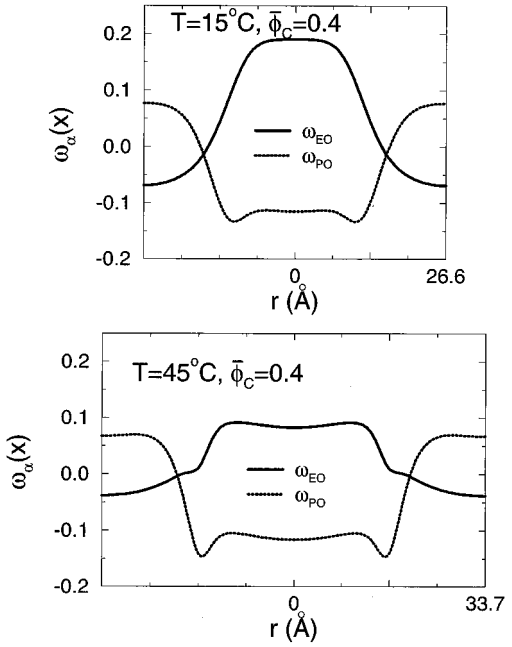

Figure 15. Mean-field potentials ω_{EO} and ω_{PO} for P94, hexagonal phase (H1), for $T = 15$ °C and $T = 45$ °C, with an overall copolymer volume fraction $\bar{\phi}_c = 0.4$.

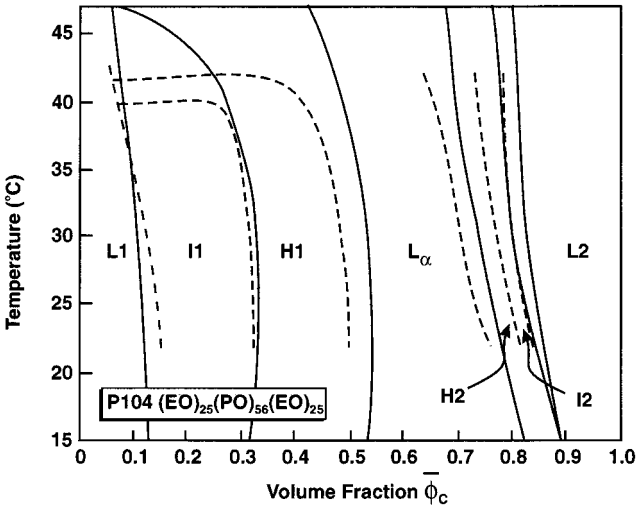

Figure 16. Phase diagram for Pluronic P104 $(EO)_{25}(PO)_{56}$-$(EO)_{25}$. The solid and dashed lines are calculated from the continuum and lattice descriptions, respectively.

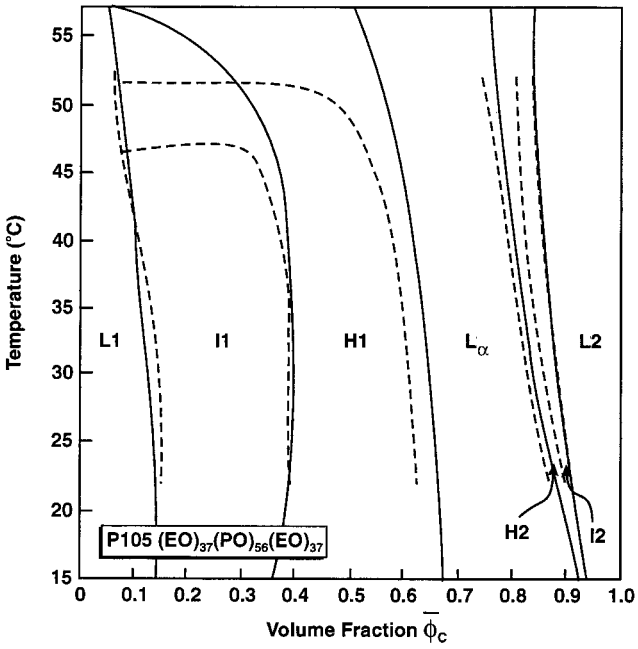

Figure 17. Phase diagram for Pluronic P105 $(EO)_{37}(PO)_{56}$-$(EO)_{37}$. The solid and dashed lines are calculated from the continuum and lattice descriptions, respectively.

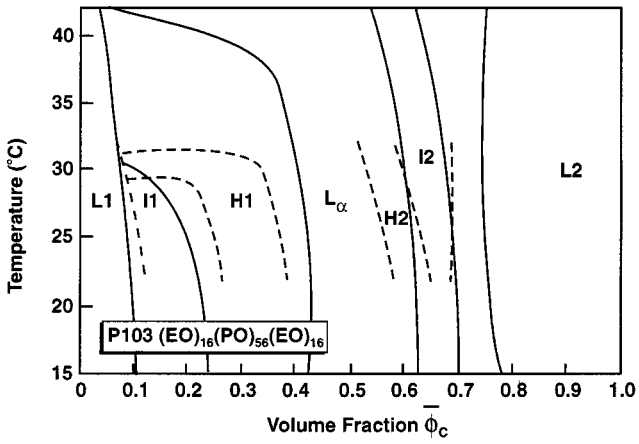

Figure 18. Phase diagram for Pluronic P103 $(EO)_{16}(PO)_{56}$-$(EO)_{16}$. The solid and dashed lines are calculated from the continuum and lattice descriptions, respectively.

EO segments is also expected, since the spontaneous curvature (defined with EO on the outside) should increase with increasing number of EO segments. For example, at 25 °C and $\bar{\phi}_c = 0.60$, the stable structure for Pluronic P104 is lamellar (L_α), whereas for Pluronic P105 at the same conditions the hexagonal phase (H1) is stable.

Figures 16−18 together with Figure 4 also make it possible to compare the results of the two models for different triblock copolymer compositions. It seems that the boundaries between the phases become more similar as the polymer length increases with constant EO/PO composition and as the number of EO segments increases with a constant number of PO segments. Thus, when at least one of the blocks becomes shorter, the agreement between the two approaches becomes worse. It seems reasonable that the two methods should give a better agreement for longer polymers, since essentially only the descriptions of the local bending of the polymers differ (cf. eqs 2 and 18 including the discussion of the λ matrix above). However, we are still not able to offer a quantitative explanation of these trends, which may be related to a different accounting of the conformational entropy contributions to the free energy in the two models at the shorter length scales.

IV. Conclusions

We have shown that the mean-field theory of triblock copolymers in a selective solvent can be used to describe the lyotropic liquid crystalline phases of the Pluronics in water, as a function of polymer concentration and temperature. Using the interaction parameters determined from binary homopolymer−water and ternary homopolymer−homopolymer−water phase diagrams, and an internal state model developed to describe the change in hydrophobic/hydrophilic behavior of the homopolymers with changing temperature,[17−24] the calculated phase diagrams are in remarkably good agreement with experiment, considering the number of simplifying assumptions made in the theory. The results from the continuum and lattice theories are very similar, except for short chains. In particular, for a

system not discussed in this paper, L64 [$(EO)_{13}(PO)_{30}$-$(EO)_{13}$], the continuum model predicts ordered phases, in agreement with experiment,[9] whereas the lattice model does not predict any ordering.

A key feature of the theoretical development is the demonstration that the complete machinery of the self-consistent mean-field theory can be used for situations where there are spatially invariant internal state energies, provided that the internal states are considered as embedded in a self-consistent potential determined by the spatial arrangement of the molecules. The resulting effective potential, including both the effect of the internal states and the local arrangement of the molecules, can then be determined by an iterative numerical procedure in the usual way.[18,25] In order to progress beyond this simplified scheme, a more realistic model where the internal state energies are affected by the local environment has to be considered. The more general scheme is analogous to the protein folding problem and is at present intractable.

The model developed in this paper should also be useful for describing ternary triblock copolymer−oil−water phase diagrams, as well as mixtures of ordered triblocks with homopolymers and small nonionic surfactants. The predicted density profiles for the different ordered phases, as a function of temperature, are amenable to studies by scattering techniques.[1] In particular, it would be interesting to see the suggested secondary structure for the higher temperatures, resulting from the increased hydrophobicilty of the EO blocks and their attempts to withdraw into the PO filled domains. Finally, the calculated density profiles have some connection to the rheological behavior of the ordered phases, although a proper description of the rheological aspects awaits the development of a model of the polymer dynamics for these complex systems.

Acknowledgment. J.N. thanks the Swedish National Science Research Council (NFR) for a grant to visit the Division of Physical Chemistry 1 at Lund University, and Professor Björn Lindman and his colleagues for their kind hospitality. P.L. acknowledges a grant from the NFR.

References and Notes

(1) Mortensen, K. *Europhys. Lett.* **1992**, *19*, 599.
(2) Zhang, K.; Khan, A. *Macromolecules* **1995**, *28*, 3807.
(3) Wanka, G.; Hoffmann, H.; Ulbricht, W. *Macromolecules* **1994**, *27*, 4145.
(4) Malmsten, M.; Lindman, B. *Macromolecules* **1992**, *25*, 5440, 5446.
(5) Alexandridis, P.; Zhou, D.; Khan, A. *Langmuir*, in press.
(6) Malmsten, M.; Linse, P.; Zhang, K.-W. *Macromolecules* **1993**, *26*, 2905.
(7) Linse, P. *Macromolecules* **1993**, *26*, 4437.
(8) Schmolka, I. R. In *Nonionic Surfactants*; Schick, M. J., Ed.; Marcel Dekker: New York, 1967; Chapter 10.
(9) Alexandridis, P.; Olsson, U.; Lindman, B. *Macromolecules* **1995**, *28*, 7700.
(10) Fredrickson, G. H.; Liu, A. J.; Bates, F. S. *Macromolecules* **1994**, *27*, 2503.
(11) Shi, A.-C.; Noolandi, J. *Macromolecules* **1995**, *28*, 3103.
(12) Doi, M.; Edwards, S. F. *The Theory of Polymer Dynamics*; Clarendon Press: Oxford, U.K., 1986; Chapter 1.
(13) Fleer, G. J.; Cohen Stuart, M. A.; Scheutjens, J. M. H. M.; Cosgrove, T.; Vincent, B. *Polymers at Interfaces*; Chapman and Hall: New York, 1993.
(14) Flory, P. J. *Principles of Polymer Chemistry*; Cornell University Press: Ithaca, NY, 1953.
(15) Hong, K. M.; Noolandi, J. *Macromolecules* **1981**, *14*, 727.
(16) Helfand, E. *J. Chem. Phys.* **1975**, *62*, 999.
(17) Karlström, G. *J. Chem. Phys.* **1985**, *89*, 4962.
(18) Linse, P.; Björling, M. *Macromolecules* **1991**, *24*, 6700.
(19) Sjöberg, Å.; Karlström, G. *Macromolecules* **1989**, *22*, 1325.
(20) Hurter, P. N.; Scheutjens, J. M. H. M.; Hatton, T. A. *Macromolecules* **1993**, *26*, 5030.
(21) Linse, P. *J. Phys. Chem.* **1993**, *97*, 13896.
(22) Linse, P. *Macromolecules* **1994**, *27*, 2685, 6404.
(23) Björling, M.; Karlström, G.; Linse, P. *J. Phys. Chem.* **1991**, *95*, 6706.
(24) Björling, M.; Linse, P.; Karlström, G. *J. Phys. Chem.* **1990**, *94*, 471.
(25) Shi, A.-C.; Noolandi, J. *Macromolecules* **1994**, *27*, 2936.
(26) Leermakers, F. A. M.; Van der Schoot, P. P. A. M.; Scheutjens, J. M. H. M.; Lyklema, J. In *Surfactants in Solution*; Mittal, K. L., Ed.; Plenum: New York, 1989; Vol. 7.
(27) van Lent, B.; Scheutjens, J. M. H. M. *Macromolecules* **1989**, *22*, 1931.
(28) Hashimoto, T.; Yamasaki, K.; Koizumi, S.; Hasegawa, H. *Macromolecules* **1993**, *26*, 2895.
(29) Hashimoto, T.; Koizumi, S.; Hasegawa, H. *Macromolecules* **1994**, *27*, 1562.
(30) Koizumi, S.; Hasegawa, H.; Hashimoto, T. *Macromolecules* **1994**, *27*, 4371.
(31) Cohen, R. E.; Torradas, J. M. *Macromolecules* **1984**, *17*, 1101.
(32) Zin, W.-C.; Roe, R.-J. *Macromolecules* **1984**, *17*, 189.
(33) Winey, K. L.; Thomas, E. L.; Fetters, L. J. *Macromolecules* **1992**, *25*, 422.
(34) Meier, D. J. In *Thermoplastic Elastomers*; Legge, N. R., Holden, G., Schroeder, H., Eds.; Hanser: Munich, 1987; Chapter 11.
(35) Matsen, M. W.; Bates, F. S. *Macromolecules* **1996**, *29*, 1091.
(36) Schmolka, I. R. *J. Biomed. Mater. Res.* **1972**, *6*, 571.

MA960272F